The tsunami warning system based on multi-array back-projection using local seismic stations

Y. Xie[1], L. Meng[1]

[1]Earth, Planetary and Space Sciences, University of California, Los Angeles, CA 90025, USA.

Corresponding author: Lingsen Meng (meng@epss.ucla.edu)

Key Points:

- We develop a tsunami warning system based on a multi-array back-projection (BP) method using local seismic networks (0.7°<Δ <3.5°).
- The multi-array BP circumvents the issue of artifact in single-array BP caused by the overlapping of multiple phases and coda waves.
- Case studies of the 2003 M8.1 Tokachi and the 2011 M9.0 Tohoku earthquakes demonstrate fast and accurate predictions for tsunami warning.

Abstract

Recent development of dense strong-motion networks and seismic array processing enables rapid tsunami predictions based on the back-projection (BP) approach. We develop a multi-array BP method using local seismic networks (0.7°<Δ <3.5°). The local BPs using individual arrays are first calculated, and are then merged into a single image of the rupture process. This multi-array approach circumvents the issue of artifact in single-array BP caused by the overlapping of multiple phases and coda waves. Based on the local BP approach, tsunami predictions are available 7 min after the origin time. Case studies of the 2003 Mw 8.1 Tokachi-oki and the 2011 Mw 9.0 Tohoku earthquakes show that the rupture zone are well resolved and are comparable with principal slip area inferred from tsunami observations. The amplitude and arrival time errors of the predicted tsunami waves are within -2.55-3.01 m and -8.7-10.0 min, which are sufficiently small for warning purposes.

Plain Language Summary

Accurate prediction of tsunami waves for residents who are close to the tsunami source requires fast characterization of tsunami-genic earthquakes. In this research, we develop a tsunami warning system based on earthquake source observations using multiple dense clusters of seismic stations installed near the coastal region. At a given stage during an earthquake, the recorded seismic wavefield are back-propagated to retrieve the direction of the seismic source with respect to each cluster of stations. By combining direction information determined at each station group, we retrieve the principle slip fault area that are most responsible for tsunami generation. A simplified earthquake source model is then constructed to predict the tsunami arrival time and height. By adopting local seismic stations within 80-400 km away from the earthquake sources, we show that the tsunami warning can be issued 7 minutes after the earthquake origin time. Our case studies of the 2003 Mw 8.1 Tokachi-oki earthquake and the 2011 Mw 9.0 Tohoku earthquake show that our approach adequately reproduces the tsunami observations. The height errors of the predicted tsunami waves are within -2.55 to 3.01 m; The errors of the arrival times are within -8.7 to 10.0 min, which are sufficiently small for warning purposes.

1 Introduction

Near-field (30 ~ 60 min after earthquake) tsunami warning in the absence of tsunami data is challenging, especially for the real-time predictions of tsunami arrival time and wave heights. Seismic waves and land-based geodetic data are generally retrieved faster than tsunamis, so they can be potentially used to construct a source model for the prediction of tsunami waves. As a first step, point source solutions are automatically derived from seismic data after an earthquake, which are used to evaluate the tsunamigenic potential of the earthquake. For instance, the W-phase solution [*Kanamori and Rivera,* 2008] determines the moment robustly based on long-period seismic body waves. Those solutions can be obtained in a short timeframe (5 ~ 10 min using regional seismic data or ~ 15 min using teleseismic data) [*Zhao et al.,* 2017; *Duputel et al.,* 2012]. The Pacific Tsunami Warning Center (PTWC) is using a similar method to carry out real-time tsunami forecast model (RIFT) of tsunami propagation for W-phase solutions with a uniform slip [*Wang et al.,* 2012]. However, this approach does not include the rupture area or the final slip distribution, and thus it is unable to make accurate site-to-site tsunami predictions. Tele-seismic data (~ 15 min after earthquake) can be inverted in real time to derive a slip model. However, such inversions suffer from non-uniqueness and impose weak constraints of the final slip distribution, leading to inaccurate predictions of tsunami waves [e.g., Lay et al., 2014; An et al., 2014]. The real-time application of the land-based GPS and strong-motion recordings has also been explored for the purpose of tsunami warning [e.g., Melgar and Bock, 2015]; Such an approach leads to a fast estimation of the fault slip distribution (< 10 min), and can be enhanced by ocean-bottom GPS sensors, which provides better constraints of slip near the trench and hence the tsunami generation.

Over the last two decades, the development of large-scale dense seismic networks, such as USArray, ORFEUS array (European network), China National Seismic Network, and Hi-net (Japanese network), has enabled rapid progresses in many fields in seismology, including the back-projection (BP) technique which images the spatial and temporal rupture process based on the wave arrivals [e.g., *Meng et al.,* 2014]. Previously, we propose a tsunami prediction approach based on the BP analysis of seismic data recorded at regional or teleseismic distances [*An and Meng,* 2016]. This approach does not depend on assumptions of prescribed fault length, width and average slip in pre-calculated tsunami scenarios, and also circumvents the non-uniqueness issue in source inversion using seismic waveforms. The required epicenter information can be provided by standard earthquake warning systems; The moment magnitude can be obtained from high-rate GPS estimations or regional W-phase inversion [*Allen et al.,* 2011, *Zhao et al.,* 2017]; The fault geometry can be extracted from the slab geometries in subduction zones [e.g., *Hayes et al.,* 2012]. The procedure is illustrated and tested for tsunamis generated by the 2011 Tohoku, 2014 Iquique and 2015 Illapel earthquakes [*An and Meng,* 2016].

For the sake of waveform simplicity and coherency, the BP-based tsunami approach originally uses regional seismic arrays (~ 10 min) or teleseismic arrays (~ 15 min). In the case of the Tohoku earthquake, the shortest warning time is achieved using regional stations. The local stations potentially provide faster warning but are excluded because the P-wave BP requires longer S-minus-P time than the rupture duration to avoid the overlapping of multiple phases. Here, in order to reduce the data collection time, we develop a multi-array S-wave BP method using seismometers at local distances (between 0.7 to 3.5 degrees). This approach first calculates source back-azimuths using individual arrays and then merges them to constrain the kinematic rupture process. We test this multi-array BP approach in a simulated real-time environment for the 2003 Mw 8.1 Tokachi-oki and the 2011 Mw 9.0 Tohoku earthquakes. The data acquisition is shortened to 100 s for S-waves recorded by local stations (~ 3.5 degrees) compared with 300 s for P-waves at regional distance (~10 degrees). Based on the local BP approach, accurate tsunami predictions are available 7 min after the origin time compared with 9 min using regional BP. Our method delivers fast tsunami warning without blind zones along the near-field coastal regions for both the Tohoku and Tokachi events. Our method sets the basis for developing an automatic procedure that provides rapid predictions of tsunami arrival times and wave heights in the near-field.

2 Methods

The array-based tsunami warning approach (Figure 1a) is briefly described as follows. First, the BP approach determines the locations of strong seismic radiations by analyzing the S-wave trains recorded by multiple local clusters of stations. In standard BP, the seismograms are filtered at high-frequencies (~1 Hz) to achieve high spatial and temporal resolutions. It has been widely recognized that seismic data with high frequency are more efficiently generated by the abrupt change in rupture speed, rather than by total large slip [e.g., *Madariaga,* 1983]. Here, we analyze the low-frequency signal (~0.02 Hz) which is more representative of the static slip and therefore tsunami generations. The seismic radiators can be regarded as the centroid locations of seismic sub-events at different stages during an earthquake. We use an ellipse that encloses the seismic radiators to approximate the rupture area. We then develop a simplified source model with uniform slip over the estimated rupture area, based on the assumption that the long-period tsunami waves are not sensitive to the detailed slip distribution [*An et al.,* 2018]. Given the rupture area S inferred from the BP result and the seismic moment M_0, the average slip, D_a can be evaluated using the definition of seismic moment $M_0 = \mu S D_a$, assuming a crustal rigidity of μ =32 GPa. To facilitate timely warning, the original array-based tsunami prediction approach indirectly infers the moment based on a scaling relation between the rupture area and seismic moment, derived for large (M 6.7 to M 9.2) subduction-zone earthquakes [*Murotani et al.,* 2013]. More accurate seismic moment of M>7.5 earthquakes can be retrieved by global W-phase solutions within 20-30 min after the event origin time using teleseismic records [*Duputel et al.,* 2012], which is too slow for the near-field tsunami predictions. Recently, rapid W-phase solutions are made available within 4 to 7 min after the event origin time using regional and local seismic data with relatively small magnitude errors (+-0.2) [*Zhao et al.,* 2017]. We envision to implement the regional W-phase inversion alongside our tsunami warning method which allows the retrieval of accurate seismic moment in a time frame comparable to the local BP operations.

Based on the principles of array back-projection (BP), we propose an algorithm to locate the sub-sources by intersecting back-azimuths of multiple arrays. First the source back-azimuths with respect to each cluster are calculated assuming plane wave arrivals. For a selected time window, we determine the source slowness vector using the correlation stacking approach. This method beamforms the cross-correlation coefficients of all station pairs to improve the robustness against scattering, multipathing and contamination of coda waves [*Frankel,* 1991; *Borcea et al.,* 2002; *Fletcher et al.,* 2006; *Meng et al.,* 2014]. The coherence function C_m for the m-th cluster and time t_0 is defined as:

$$C_m(t_0,\theta) = \sum_{ij} cc_{ij}(t_0,\theta) = \sum_{ij} \frac{\sum_{t=t_0-t1/2}^{t=t_0+t1/2} x_i(t-\tau_i(\theta))x_j(t-\tau_j(\theta))}{\sum_{t=t_0-t1/2}^{t=t_0+t1/2} x_i(t)^2 x_j(t)^{2\,1/2}} \quad (1)$$

where i and j are the station index. cc_{ij} is the correlation coefficient between two stations. x_i is the seismogram. t_0 is the time after the origin time. $\tau_i(\theta)$ is the time delay compared to a reference station assuming the slowness vector is θ. The sums in the equations are computed in a running time window of length t_1 centered at t_0. We perform a grid search of the slowness vector and identify the back-azimuth corresponding to the peak stacked coherence.

The second step is to locate the seismic radiators by intersecting the back-azimuths in the source area (Figure 1b). For each cluster, the possible source locations are along a vector pointing from the center of the cluster towards the back-azimuth. We apply a Gaussian smoothing to this source location vector accounting for the uncertainty of the back-azimuths. The joint spatial probability distribution of the source location determined with multiple arrays is given by:

$$p(i,j,t) = \sum_{k=1}^{n} \exp\left[\frac{\theta_{t_k}(i,j) - \theta_{m_k}\left(t + t_{0_k}\right)}{(2\sigma_k)^2}\right] \quad (2)$$

where i and j are the grid index and k is the cluster index. t is the time after the origin time. p is the probability of the existence of a seismic radiator. n is the number of clusters. σ_k is the Gaussian smoothing factor. We use $\sigma_k = 10°$ after examining the uncertainties of the back-azimuths of a M

5.5 reference earthquake (Text S1). θ_{t_k} and θ_{m_k} are the theoretical and measured back-azimuth, respectively. t_{0_k} is the theoretical arrival time of S wave at the reference station, which is calculated using the PREM model [*Dziewonski and Anderson,* 1981]. The source grid with the highest probability is considered as the location of the radiator at a time step.

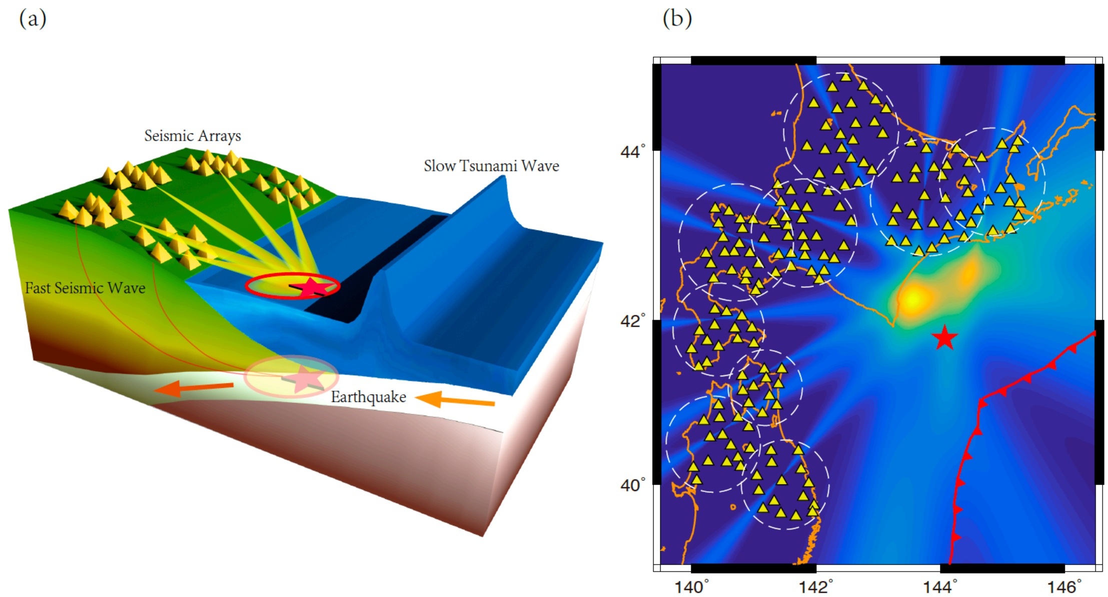

Figure 1 (**a**) Sketch of tracking tsunami-genic earthquakes with multi-array back-projection method. The seafloor motion excites the tsunami wave during a megathrust earthquake that occurred at the subduction interface. The red stars represent the hypocenter and epicenter. The earthquake rupture area (red ellipse) is imaged by the local onshore seismic networks (yellow tetrahedrons). (**b**) The snapshot of the multi-array back-projection image. The background color indicates the joint spatial probability distribution of the source location 40 seconds after the origin time of the M 8.1 Tokachi earthquake determined with multiple arrays BP analysis using 9 clusters from the Hi-net stations (yellow triangles). The red star is the epicenter.

We envision that the BPs will be applied automatically to the continuous recording in real-time. It's therefore essential to identify the beginning and the end of the earthquake. We assume that the origin time of the earthquake is provided by the standard EEW system. The end of the earthquake can be described by the spatial scattering of the successive radiators. During the earthquake, the seismic radiators are focused in space due to coherent S-wave arrivals. At the end of the earthquake, the radiators become scattered due to the dominance of the coda waves (Figure S1 and Figure S2). An earthquake can be considered to have ended when the spatial variance of the radiators exceeds the maximum possible separations within a time window (Text S2).

Once the locations of seismic radiators are determined, we construct a simplified source model for tsunami forward simulation. First we estimate the rupture zone by enclosing the radiators with an ellipse using the confidence interval algorithm (Text S3 and Figure S2) and measure the area of the ellipse, S_{bp}. Since the low-frequency (~0.02 Hz) BP radiators represent centroid locations of seismic sub-sources, we assume that the "asperities" (area of large slip) dominate the tsunami generation and the contributions of low-slip rupture area can be ignored in the tsunami wave simulation. The large slip area is similar to the "asperity" concept proposed in Murotani et al., [2013] (source area with slip larger than 1.5 times of the average slip). Then we determine the average slip inside the BP-inferred area, D_{bp}. The average slip on the total source area, D can be inferred based on seismic moment and the whole rupture area, S. To estimate D_{bp}, we establish an empirical relation between the degree of slip concentration (D_{bp}/D) versus normalized source area (S_{bp}/S), based on slip models of 8 historical tsunamigenic megathrust earthquakes (Figure S3). we find that for the Tohoku and Tokachi earthquakes, S_{bp}/S ~ 0.145 and D_{bp}/D ~ 2.88. Based on this relation, the total area S is first estimated using the BP-inferred area S_{bp}. Then using the seismic moment estimated from the W-phase, the average slip D is calculated according to the definition of seismic moment $M_0 = \mu SD$, assuming the rigidity of the fault zone rock is 32 GPa. Then, we construct a uniform slip model assuming that the slip over the BP source area D_{bp} is 2.88 times of the average slip D. Finally, we conduct a tsunami simulation to predict the amplitudes and arrival times of the tsunami waves.

3 Application

3.1 The 2003 Mw 8.1 Tokachi earthquake

Our local-array-based warning system is applied in a simulated real-time fashion to the 2003 Mw 8.1 Tokachi-oki event and the 2011 Mw 9.0 Tohoku event. For the Tokachi event, we use 13 circular seismic clusters with epicentral distances smaller than 3.5 degrees, 7 of which are constructed from the K-net strong motion stations and 6 from the Hi-net stations (Figure 2a and Figure S4a). Each cluster is between 1.0-1.9 degrees in diameter. The size is empirically chosen to balance the waveform coherency, the plane wave assumption and the resolution of back-projection. The station spacings are between 11 - 15 km for the K-net and 15 - 55 km for the Hi-net. We adopt the transverse component to enhance the signal of the S wave and filter the waveforms to a low-frequency band of 0.02 - 0.1 Hz for Hi-Net stations and 0.01 - 0.07 Hz for K-net stations. Only the Hi-net stations are used to image the initial stage of the rupture process, because the initial S-waves did not reach the triggering threshold of the strong-motion accelerometers (The triggering time ranges from 27 s to 68 s after the S-wave arrival depending on the stations in K-net).

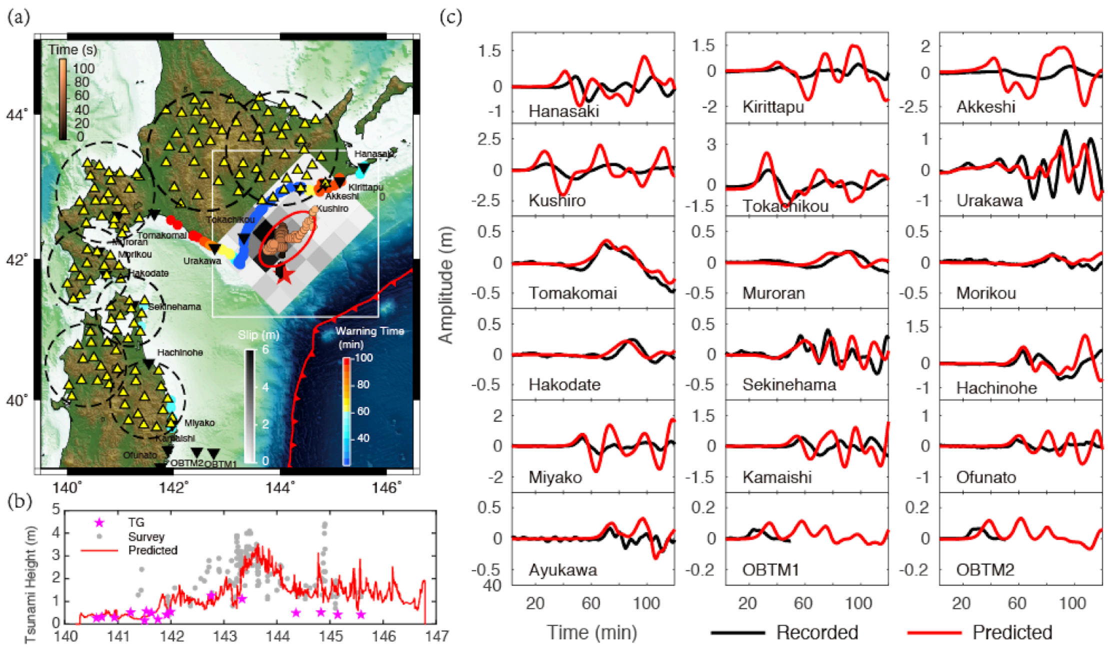

Figure 2 The case study of the 2003 Mw 8.1 Tokachi-oki earthquake. (**a**) The brownish circles are back-projection radiators color-coded by time and sized by the normalized power. The red eclipse encloses estimated 'asperity' region; The red star is the epicenter and yellow triangles are strong motion stations. Black triangles are tsunami stations. The dashed black circles mark the clusters of stations used for the array analysis. The warning time (color circles along the coast) is estimated from the arrival time observed by *Tanioka et al.,* [2004]. The greyish tiles are the slip distribution estimated with tsunami data [Romano et al., 2010]. The source region in the white box is shown in Figure S5; (**b**) The runup heights estimated from the elliptical source model (red) and from a post-tsunami survey (grey dots) [*Tanioka et al.,* 2004]. The magenta stars denote the peak amplitudes at the coastal tsunami stations; (**c**) The measurement (black) and tsunami waveform (red) predicted by the simplified rupture model.

We perform the correlation stacking approach (equation (1)) to the Tokachi earthquake recordings with a 30-second sliding window to calculate the back-azimuths. This relatively long window corresponds to the relatively long-period filter we apply to the data. Then equation (3) is used to intersect the back-azimuths of individual clusters and identify the seismic radiators, shown as colored circles in figure 2a. The locations of the seismic radiators agree well with the principal slip zone defined by a finite fault inversion model using tsunami waves [*Romano et al.,* 2010]. The time span of coherent BP is about 118 s, which exceeds the reported earthquake duration of 50 s based on the finite fault solutions [*Yagi,* 2004; *Yamanaka and Kikuchi,* 2003]. This apparent longer duration is possibly due to the long-period S and Love phases after applying the low-frequency filter. The area of the fitted ellipse S_{bp} is 4948 km^2, which corresponds to an average slip D_{bp} of 6.03 m, given the W-phase moment magnitude of Mw 8.16 from USGS. These estimations agree with the source area of the largest slip in the Romano model, with an S_{bp} area (area of all the grids with slip larger than 2.88 times of the average slip) of about 4629 km^2 and an average slip D_{bp} of 4.05 m. The estimated total rupture area is about 31925 km^2, which is very close to that in the Romano model, 31000 km^2.

Using the prescribed fault surface based on the Slab 2.0 model (strike = 210°, dip = 19.5°) and assuming a rake angle of 90°, the source model with uniform slip distribution is implemented to predict the tsunami waves, using the COMCOT v1.7 package [*Liu et al.,* 1998; *Wang and Liu,* 2006, 2007]. The amount of warning times (colored circles along the coast line on figure 2a) are greater than 20 min using our approach. We compare our predictions with recordings at 16 coastal tsunami stations and 2 ocean bottom tsunami-meters in Hokkaido and northern Honshu. The average errors of the predicted arrival times and amplitudes are 3.34 min and 0.27 m, respectively. At 80% of the stations, the arrival time and amplitude errors are smaller than 3.42 min and 0.76 m, respectively, which achieves sufficient accuracy for warning purpose.

3.2 The 2011 Mw 9.0 Tohoku earthquake

The proposed methodology is also applied to the tsunami generated by the 2011 Tohoku earthquake. We use 10 clusters of the K-net strong motion stations and 4 clusters of the Hi-net stations (Figure 3a and Figure S4b). The diameters of the clusters are approximately 1-1.6 degrees. All stations are in north Honshu with epicentral distances smaller than 3.5 degrees. We conduct the local-array-based BP using the same parameters as the Tokachi earthquake. The inferred seismic radiators are shown as the colored circles in Figure 3a. The time duration for BP is about 154 s, which is grossly comparable to other BP studies using teleseismic stations or local strong motion network [*Kiser and Ishii,* 2012; *Meng et al.,* 2011; *Maercklin et al.,* 2012; *Honda et al.,* 2011]. The inferred source region is consistent with the principle slip zone in the finite fault inversion model based on tsunami recordings [*Fujii et al.,* 2011]. The estimated S_{bp} is 14358 km^2. Based on the moment magnitude of Mw 9.1 determined by USGS W-phase solution, the average slip D_{bp} is 35.4 m. In comparison, the S_{bp} and D_{bp} estimated from the model of *Satake et al.* [2013] are 13927 km^2 and 35.1 m, respectively.

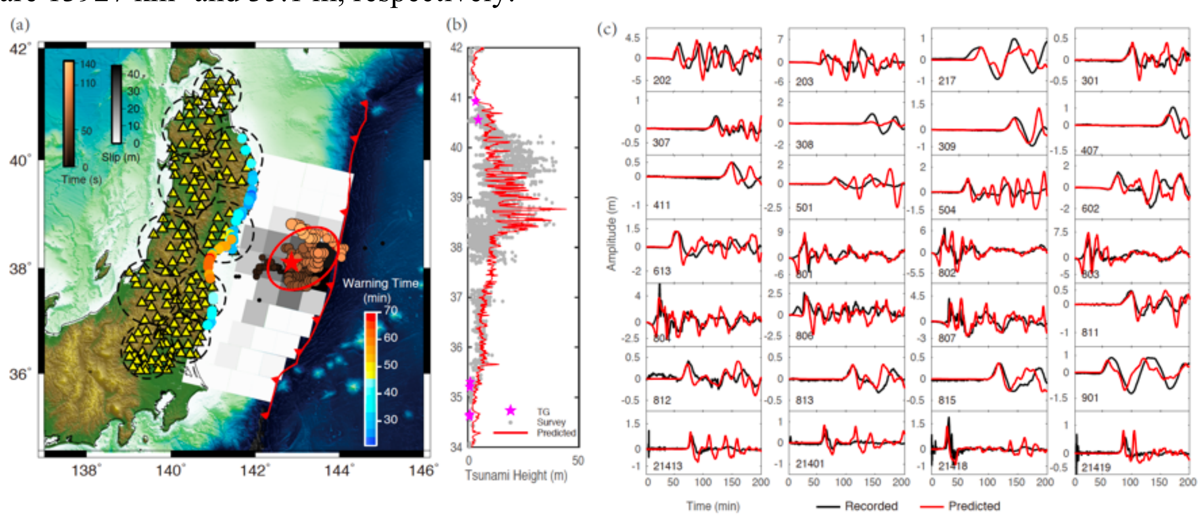

Figure 3 The case study of the 2011 Mw 9.0 Tohoku event. (**a**) The brownish circles are back-projection radiators color-coded by time and sized by the normalized power. The red eclipse encloses estimated 'asperity' region; The red star is the epicenter and yellow triangles are strong motion stations. The dashed black circles mark the clusters of stations used for the array analysis. The warning time (color circles along the coast) is estimated from the arrival time observed by *Muhari et al.* [2012]. The greyish tiles are the slip distribution estimated with tsunami data [*Fujii et al.,* 2011]. (**b**) The runup heights estimated from the elliptical source model (red) and from a post-tsunami survey (grey dots) [*Mori et al.,* 2011]. The magenta stars denote the peak amplitudes

at the coastal tsunami stations; (**c**) The measurement (black) and tsunami waveform (red) predicted by the simplified rupture model.

A uniform slip model is then constructed in order to predict the tsunami waves using COMCOT. We compare our predictions with 28 tsunami recordings (The map of the distribution of the stations is in Figure S6). The average errors of the predicted arrival times and amplitudes are 2.20 min and 0.58 m, respectively. The arrival time and amplitude errors at 80% stations are smaller than 3.14 min and 0.84 m, which is reasonably small for the warning purpose. The runup heights are underestimated for the coastal region from 39.5° N to 40° N. A possible second tsunami source near the trench around 39.5 ˚N [*Satake et al.,* 2013] may contribute to the largest tsunami heights observed along the Sanriku coast.

4 Discussion

The case studies of the Tokachi-oki and Tohoku earthquakes allow us to assess the performance of the simplified source model in predicting tsunami generations. First, since the multi-array approach uses a low frequency band (0.02-0.1 Hz and 0.01-0.07 Hz), we are explicitly assuming that the "asperities" (source areas of large slip) are responsible for the tsunami generation. This assumption seems to provide better tsunami predictions than the uniform slip models over the entire rupture area explored in our previous work [*An and Meng,* 2016]. In our case studies, this asperity model successfully captures the decay of the run-up height along the coastline as a function of the epicentral distance. In comparison, the runup heights predicted by uniform slip models over the whole rupture area are underestimated close to the epicenter and overestimated away from the epicenter [*An and Meng,* 2016]; Another simplification is that the 3D velocity variation is not considered when the S-wave arrival times are calculated. Moreover, the radiators are achieved assuming the theoretical back-azimuths are along the great circle path, which ignores the ray path distortion due to lateral velocity variation. These problems are partially mitigated by our strategy of combining multiple clusters, which bears some tolerance on the back-azimuth errors [*Fan et al.,* 2018]. In our future work, we will test if the local 3D velocity model improves the location accuracy of the BP radiators [*Liu et al.,* 2017]. We will pre-calculate such travel-time tables and corrections for back-azimuth errors for target source regions to facilitate real-time BP. Alternatively, empirical correction can be applied to improve the accuracy of the BP radiators [*Ishii et al.,* 2007; *Meng et al.,* 2014; *Meng et al.,* 2016a]. In *An and Meng* [2016], a static correction to the back azimuths is applied based on the difference between the theoretical back-azimuths of the hypocenter of the Tohoku earthquake and the observed back-azimuths measured with the initial phase arrivals. This bias is about 10 degrees for the Kyushu array and is possibly caused by the lateral velocity contrast between the island arc and the back-arc basin. We do not apply this correction in this study because the initial seismic recordings at strong motion stations are not available.

The proposed warning system achieves reasonable predictions of tsunami waves (Figure 4). The errors of the amplitudes and arrival times range from -2.55 to 3.01 m and -8.7 to 10.0 min for all tsunami stations, respectively. The errors at 60% of the stations are less than 2.71 min in arrival times and 0.23 m in amplitudes. This level of errors is close to the predictions using high-rate GPS data [*Melgar and Bock,* 2013], which is reasonably small for tsunami early warning purpose. Most of the arrival time errors can be accounted by the limited resolution of the bathymetry data used in the tsunami forward simulation. For example, the predicted arrival time is about 8 min earlier than the measurement at the station Akkeshi. Using the 15 arcsec bathymetry data, we have to move the station for 1500 m to make it in a wet grid in the wave propagation simulation, which results in about 4.5 min error for the arrival time considering that the water depth of this region is about 3 m and the tsunami wave velocity is 5.5 m/s. Another source of error is the uncertainty of the source locations. For the Tokachi event, the radiators roughly cover the peak slip region, but shift to the east by about 20 km (Figure S5), which leads to less than 1.7 min error of the arrival time considering that the water depth is about 4 km near the source and the tsunami wave velocity is 200 m/s.

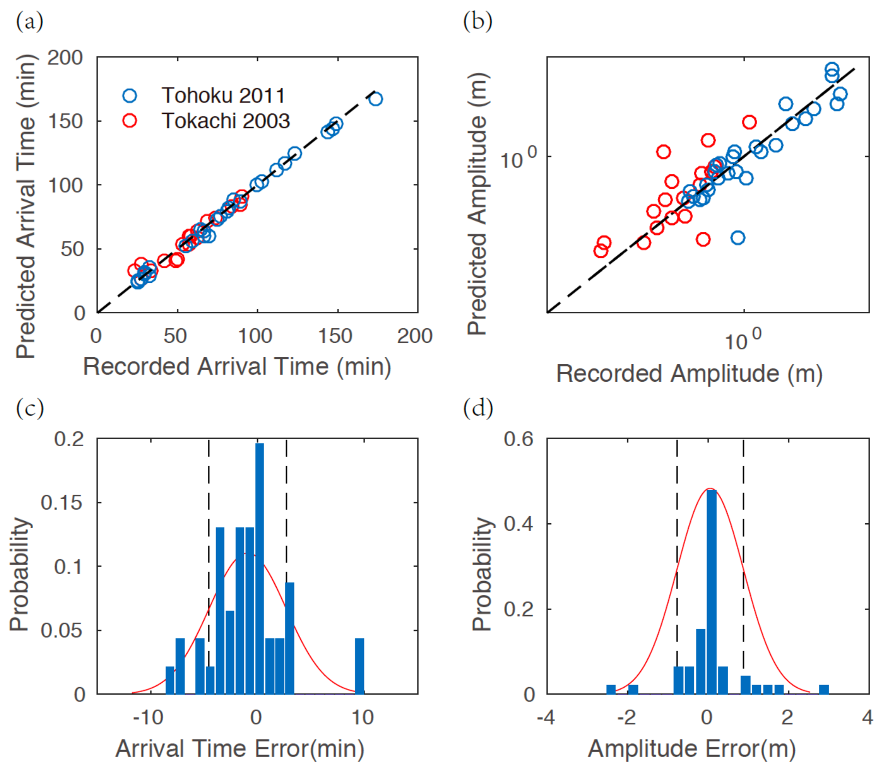

Figure 4 Errors of predicted arrival time and amplitude at all tsunami stations for the Tohoku and Tokachi earthquakes. (**a**) Predicted and recorded arrival time; (**b**) Predicted and recorded amplitude; (**c**) Arrival time error distributions; (**d**) Amplitude error distributions. The red curves are the fitted probability density using a Gaussian distribution. The dashed lines mark the region within the standard deviation.

The runup heights are underestimated in both case studies. For the Tohoku event, the runup heights from 39.5° N to 40° N are significantly underestimated. *Satake et al.,* [2013] use 53 tsunami stations to invert for the slip model. Their result indicates that a delayed shallow rupture with a 10 m slip is responsible for the maximum tsunami heights measured on the Sanriku coast. In our approach, the later rupture in the south of principal-slip area is missing, which may be masked by the love wave of the previous sub-sources [*Maercklin et al.,* 2012]. In this scenario, the seismic radiation of the rupture on splay faults is also masked by the plate-interface rupture and is hence not able to be picked up by the BP method, which leads to the underestimation of the elevated run-up near Sanriku. Besides, the inundation is sensitive to the topography and bathymetry near the coast. The runup heights predicted from the slip model of *Satake et al.* [2013] fit the observations very well, using the digital bathymetry charts (M7000 series) provided by MIRC, which has a resolution of 5 arcsec near the coast. *Shimozono et al.* [2012] investigate the inundation characteristics of the 2011 Tohoku event on the central Sanriku coast and find that the tsunami height has positive dependency on topographic slopes and significant variations along the coastline. They also propose that compared to the U-shape bays, the V-shape bays suffer from the funnel effect and local wave resonances more, which contributes to the observed extreme heights. Suppasri et al. [2016] reviewed the improvements of tsunami simulations including using fine topographical data with resolution of 5 m. Thus, the underestimation of tsunami height of our method is partially caused by missing a possible secondary tsunami source and by the coarse bathymetry (30 or 15 arc-seconds), which limits the capability of predicting the complicated wave behavior near the coast.

The first reliable W-phase inversion can be obtained using regional stations (5-6 degrees) within 3 min for the Tohoku event [*Zhao et al.,* 2017]. Assuming that the data process costs 2 minutes, the propagation of S waves takes about 100 s and that the rupture duration of the earthquake is 3 min, the warning system can issue the warning 7 minutes after the initial rupture of the Tohoku earthquake. Compared to regional seismic arrays (9 min) and teleseismic arrays (19 min) [*An and Meng,* 2016], the warning time is significantly shortened because the local seismic data are collected faster. The warning time is comparable to the method using high-rate GPS waveforms and strong motion data (< 10 min) [*Melgar and Bock,* 2015; *Melgar et al.,* 2016a] and slower than the widely implemented method using a pre-calculated database (The initial warning is issued 3 min after the origin time by JMA in the Tohoku event [*Hoshiba and Ozaki,* 2014]). The warning systems based on the tsunami observations are more reliable but require a dense tsunami array. *Yamamoto et al.* [2016a] proposed a real-time tsunami forecast system by matching the offshore pressure data recorded by the cabled network, S-net with the pre-calculated tsunami height spatial distributions. They also develop a method to constrain the centroid location of tsunami source using S-net within several minutes [2016b]. In Figure 2a and 3a, we show the theoretical warning time of the local-array approach estimated by subtracting 7 minutes from the measured arrival times of tsunami waves [*Tanioka et al.,* 2004; *Muhari et al.,* 2012]. None of the coastline falls in the blind zone. The minimum warning times are 21 min and 16 min for the Tokachi and Tohoku events, respectively. The proposed warning system is also easy to be implemented. The seismic clusters can be designed or pre-selected among existing network for regions prone to high tsunami risks. The BP and tsunami waveform prediction process can be fully automated without human interventions. The proposed warning system is a compensation to the current warning systems. A combination with early warning approaches based on W-phase and high-rate GPS can potentially reduce the uncertainty and provide a more reliable outcome.

5 Conclusions

We developed an array-based tsunami warning approach that predicts tsunami arrival time and wave heights based on rapid earthquake source characterization through back-projections (BP) of seismic arrays at local distance (0.7 to 3.5 degrees). The back-azimuths retrieved by individual arrays are combined to estimate locations of low-frequency (0.01-0.1 Hz) seismic radiators. This multiple-array back-projection scheme mitigates the artifacts due to overlapping multiple phases and coda waves, and reduces the source location uncertainties due to 3D travel-time errors. The local BP observations allow to construct uniform-slip models enclosing the “asperity” (area of large slip), which are the most responsible for tsunami generation. We also develop an empirical scaling relation to determine the slip of the asperity model, and an automatic procedure to determine the end of an earthquake in continuous seismic recordings. We apply the array-based tsunami warning approach to the 2003 M 8.1 Tokachi-oki earthquake and the 2011 M 9.0 Tohoku earthquake in a simulated real-time environment utilizing 13-14 local clusters of strong motion stations or broadband stations. The test results show that the asperity model is an effective approximation of the tsunami source and produces reasonably small error of arrival times and amplitudes for warning purposes. This approach provides an independent perspective of evaluating low frequency seismic sources in real-time and achieves tsunami prediction in 7 minutes, significantly faster than previous array-based warning approach using regional and teleseismic recordings, which has the potential to be integrated into the current tsunami warning systems.

Acknowledgments

This work is supported by NSF Geophysics grant EAR-1833532, NSF CAREER grant EAR-1848486, by the Leon and Joanne V.C. Knopo 481 Fund. We thank the General Bathymetric Chart of the Oceans (www.gebco.net) for providing high resolution bathymetry data, Sea Level Station Monitoring Facility, Intergovernmental Oceanographic Commission of UNESCO (www.ioc-sealevelmonitoring.org) for providing the tide gauge data, NOAA Center for Tsunami Research (https://nctr.pmel.noaa.gov/Dart/) for providing DART data, and the Japanese National Research Institute for Earth Science and Disaster Prevention (NIED) for providing the broadband and strong-motion seismic recordings (http://www.hinet.bosai.go.jp; http://www.kyoshin.bosai.go.jp/). We appreciate the authors of the COMCOT software package (http://223.4.213.26/archive/tsunami/ cornell/comcot down.htm). We thank Chao An, Tungcheng Ho and Fabrizio Romano for valuable discussions about tsunami wave propagation simulation. We thank Anawat Suppasri for providing their measured arrival time data of Tohoku event. We thank Shunsuke Takemura for his help with the Hi-net data before 2004. We thank Vincent Spruyt for his codes of estimating the covariance error ellipse (https://www.visiondummy.com/2014/04/draw-error-ellipse-representing-covariance-matrix/#Source_Code).

References

Allen, R. M., & Ziv, A. (2011). Application of real- time GPS to earthquake early warning.Geophysical Research Letters,38(16).

An, C., Sepúlveda, I., & Liu, P. L. F. (2014). Tsunami source and its validation of the 2014 Iquique, Chile, earthquake. Geophysical Research Letters, 41(11), 3988-3994.

An, C., & Meng, L. (2016). Application of array backprojection to tsunami prediction and early warning. Geophysical Research Letters, 43(8), 3677-3685.

An, C., Liu, H., Ren, Z., & Yuan, Y., (2018). Prediction of Tsunami Waves by Uniform Slip Models. Journal of Geophysical Research: Oceans.

Borcea, L., Papanicolaou, G., Tsogka, C., & Berryman, J. (2002). Imaging and time reversal in random media. Inverse Problems, 18(5), 1247.

Duputel, Z., Kanamori, H., Tsai, V. C., Rivera, L., Meng, L., Ampuero, J. P., & Stock, J. M. (2012). The 2012 Sumatra great earthquake sequence. Earth and Planetary Science Letters, 351, 247-257.

Dziewonski, A. M., and D. L. Anderson. 1981. "Preliminary reference Earth model." Phys. Earth Plan. Int. 25:297-356.

Fan, W., de Groot-Hedlin, C. D., Hedlin, M. A., & Ma, Z. (2018). Using surface waves recorded by a large mesh of three-element arrays to detect and locate disparate seismic sources. Geophysical Journal International, 215(2), 942-958.

Fletcher, J. B., Spudich, P., & Baker, L. M. (2006). Rupture propagation of the 2004 Parkfield, California, earthquake from observations at the UPSAR. Bulletin of the Seismological Society of America, 96(4B), S129-S142.

Frankel, A. (1991). High- frequency spectral falloff of earthquakes, fractal dimension of complex rupture, b value, and the scaling of strength on faults. Journal of Geophysical Research: Solid Earth, 96(B4), 6291-6302.

Fujii, Y., & Satake, K. (2007). Tsunami source of the 2004 Sumatra–Andaman earthquake inferred from tide gauge and satellite data. Bulletin of the Seismological Society of America, 97(1A), S192-S207.

Fujii, Y., Satake, K., Sakai, S. I., Shinohara, M., & Kanazawa, T. (2011). Tsunami source of the 2011 off the Pacific coast of Tohoku Earthquake. Earth, planets and space, 63(7), 55.

Fujii, Y., & Satake, K. (2013). Slip distribution and seismic moment of the 2010 and 1960 Chilean earthquakes inferred from tsunami waveforms and coastal geodetic data. Pure and Applied Geophysics, 170(9-10), 1493-1509.

Hayes, G. P., Wald, D. J., & Johnson, R. L. (2012). Slab1. 0: A three- dimensional model of global subduction zone geometries. Journal of Geophysical Research: Solid Earth, 117(B1).

Honda, R., Yukutake, Y., Ito, H., Harada, M., Aketagawa, T., Yoshida, A., ... & Kimura, H. (2011). A complex rupture image of the 2011 off the Pacific coast of Tohoku Earthquake revealed by the MeSO-net. Earth, planets and space, 63(7), 13.

Hoshiba, M., & Ozaki, T. (2014). Earthquake Early Warning and Tsunami Warning of the Japan Meteorological Agency, and Their Performance in the 2011 off the Pacific Coast of Tohoku Earthquake Mw 9.0. In Early Warning for Geological Disasters (pp. 1-28). Springer, Berlin, Heidelberg.

Ishii, M., Shearer, P. M., Houston, H., & Vidale, J. E. (2007). Teleseismic P wave imaging of the 26 December 2004 Sumatra- Andaman and 28 March 2005 Sumatra earthquake ruptures using the Hi- net array. Journal of Geophysical Research: Solid Earth, 112(B11).

Johnson, J. M., Tanioka, Y., Ruff, L. J., Satake, K., Kanamori, H., & Sykes, L. R. (1994). The 1957 great Aleutian earthquake. In Shallow Subduction Zones: Seismicity, Mechanics and Seismic Potential (pp. 3-28). Birkhäuser Basel.

Johnson, J. M., Satake, K., Holdahl, S. R., & Sauber, J. (1996). The 1964 Prince William Sound earthquake: Joint inversion of tsunami and geodetic data. Journal of Geophysical Research: Solid Earth, 101(B1), 523-532.

Johnson, J. M., & Satake, K. (1999). Asperity distribution of the 1952 great Kamchatka earthquake and its relation to future earthquake potential in Kamchatka. In Seismogenic and Tsunamigenic Processes in Shallow Subduction Zones (pp. 541-553). Birkhäuser, Basel.

Kanamori, H., & Rivera, L. (2008). Source inversion ofWphase: speeding up seismic tsunami warning. Geophysical Journal International, 175(1), 222-238.

Kiser, E., & Ishii, M. (2012). The March 11, 2011 Tohoku- oki earthquake and cascading failure of the plate interface. Geophysical Research Letters, 39(7).

Lay, T., Yue, H., Brodsky, E. E., & An, C. (2014). The 1 April 2014 Iquique, Chile, Mw 8.1 earthquake rupture sequence. Geophysical Research Letters, 41(11), 3818-3825.

Liu, P. L., Woo, S. B., & Cho, Y. S. (1998). Computer programs for tsunami propagation and inundation. Cornell University, 25.

Liu, Z., Song, C., Meng, L., Ge, Z., Huang, Q., & Wu, Q. (2017). Utilizing a 3D global P- wave tomography model to improve backprojection imaging: A case study of the 2015 Nepal earthquake. Bulletin of the Seismological Society of America, 107(5), 2459-2466.

Madariaga, R. (1983). High frequency radiation from dynamic earthquake. Ann. Geophys., 1, 17.

Maercklin, N., Festa, G., Colombelli, S., & Zollo, A. (2012). Twin ruptures grew to build up the giant 2011 Tohoku, Japan, earthquake. Scientific reports, 2, 709.

Melgar, D., & Bock, Y. (2013). Near- field tsunami models with rapid earthquake source inversions from land- and ocean- based observations: The potential for forecast and warning. Journal of Geophysical Research: Solid Earth, 118(11), 5939-5955.

Melgar, D., & Bock, Y. (2015). Kinematic earthquake source inversion and tsunami runup prediction with regional geophysical data. Journal of Geophysical Research: Solid Earth, 120(5), 3324-3349.

Melgar, D., Allen, R. M., Riquelme, S., Geng, J., Bravo, F., Baez, J. C., ... & Bevis, M. (2016). Local tsunami warnings: Perspectives from recent large events. Geophysical Research Letters, 43(3), 1109-1117.

Meng, L., Inbal, A., & Ampuero, J. P. (2011). A window into the complexity of the dynamic rupture of the 2011 Mw 9 Tohoku- Oki earthquake. Geophysical Research Letters, 38(7).

Meng, L., Allen, R. M., & Ampuero, J. P. (2014). Application of seismic array processing to earthquake early warning. Bulletin of the Seismological Society of America, 104(5), 2553-2561.

Meng, L., Zhang, A., & Yagi, Y. (2016a). Improving back projection imaging with a novel physics- based aftershock calibration approach: A case study of the 2015 Gorkha earthquake. Geophysical Research Letters, 43(2), 628-636.

Mori, N., Takahashi, T., Yasuda, T., & Yanagisawa, H. (2011). Survey of 2011 Tohoku earthquake tsunami inundation and run- up. Geophysical research letters, 38(7).

MUHARI, A., IMAMURA, F., SUPPASRI, A., & MAS, E. (2012). Tsunami arrival time characteristics of the 2011 East Japan Tsunami obtained from eyewitness accounts, evidence and numerical simulation. Journal of Natural Disaster Science, 34(1), 91-104.

Murotani, S., Satake, K., & Fujii, Y. (2013). Scaling relations of seismic moment, rupture area, average slip, and asperity size for M~ 9 subduction- zone earthquakes. Geophysical Research Letters, 40(19), 5070-5074.

Romano, F., Piatanesi, A., Lorito, S., & Hirata, K. (2010). Slip distribution of the 2003 Tokachi-oki Mw 8.1 earthquake from joint inversion of tsunami waveforms and geodetic data. Journal of Geophysical Research: Solid Earth, 115(B11).

Satake, K., Fujii, Y., Harada, T., & Namegaya, Y. (2013). Time and space distribution of coseismic slip of the 2011 Tohoku earthquake as inferred from tsunami waveform data. Bulletin of the seismological society of America, 103(2B), 1473-1492.

Shimozono, T., Sato, S., Okayasu, A., Tajima, Y., Fritz, H. M., Liu, H., & Takagawa, T. (2012). Propagation and inundation characteristics of the 2011 Tohoku tsunami on the central Sanriku coast. Coastal engineering journal, 54(01), 1250004.

Suppasri, A., Latcharote, P., Bricker, J. D., Leelawat, N., Hayashi, A., Yamashita, K., ... & Imamura, F. (2016). Improvement of tsunami countermeasures based on lessons from the 2011 Great East Japan earthquake and tsunami—Situation after five years. Coastal Engineering Journal, 58(4), 1640011-1.

Tanioka, Y., Nishimura, Y., Hirakawa, K., Imamura, F., Abe, I., Abe, Y., ... & Harada, K. (2004). Tsunami run-up heights of the 2003 Tokachi-oki earthquake. Earth, planets and space, 56(3), 359-365.

Wang, X., & Liu, P. L. F. (2006). An analysis of 2004 Sumatra earthquake fault plane mechanisms and Indian Ocean tsunami. Journal of Hydraulic Research, 44(2), 147-154.

Wang, X., & Liu, P. L. F. (2007). Numerical simulations of the 2004 Indian Ocean tsunamis—coastal effects. Journal of Earthquake and Tsunami, 1(03), 273-297.

Wang, D., Becker, N. C., Walsh, D., Fryer, G. J., Weinstein, S. A., McCreery, C. S., ... & Duputel, Z. (2012). Real- time forecasting of the April 11, 2012 Sumatra tsunami. Geophysical Research Letters, 39(19).

Yagi, Y. (2004). Source rupture process of the 2003 Tokachi-oki earthquake determined by joint inversion of teleseismic body wave and strong ground motion data. Earth, planets and space, 56(3), 311-316.

Yamamoto, N., Hirata, K., Aoi, S., Suzuki, W., Nakamura, H., & Kunugi, T. (2016a). Rapid estimation of tsunami source centroid location using a dense offshore observation network. Geophysical Research Letters, 43(9), 4263-4269.

Yamamoto, N., Aoi, S., Hirata, K., Suzuki, W., Kunugi, T., & Nakamura, H. (2016b). Multi-index method using offshore ocean-bottom pressure data for real-time tsunami forecast. Earth, Planets and Space, 68(1), 128.

Yamanaka, Y., & Kikuchi, M. (2003). Source process of the recurrent Tokachi-oki earthquake on September 26, 2003, inferred from teleseismic body waves.Earth, Planets and Space, 55(12), e21-e24.

Zhao, X., Duputel, Z., & Yao, Z. (2017). Regional W- Phase Source Inversion for Moderate to Large Earthquakes in China and Neighboring Areas.Journal of Geophysical Research: Solid Earth, 122(12).